Variational Treatment of the Diffraction at the Facet of d.h. Lasers and of Dielectric Millimeter Wave Antennas

TULLIO E. ROZZI, SENIOR MEMBER, IEEE, AND GERARD H. IN'T VELD

Abstract—**This paper presents an accurate variational treatment of the diffraction of TE and TM waves by an abrupt transverse discontinuity in a dielectric waveguide, such as the mirror of a double heterostructure (d.h.) injection laser, or the end plane of a dielectric slab antenna for millimeter waves, under the assumption of small aspect ratio.**

A matrix representation of the Green's function is derived analytically, in the limit of small effective frequency, for the TE case. For the TM case, the complication introduced by the discontinuity of the transverse electric field across the dielectric interface is discussed in detail.

The numerical examples refer to the d.h. laser configuration. Both transverse directions (perpendicular as well as parallel) to the junction are studied. The effect of mode coupling at the mirror of a LOC laser as well as the effect of an antireflection coating are investigated.

I. Introduction

THE PROBLEM OF diffraction of surface waves at the end facet of a double heterostructure (d.h.) laser (Fig. 1(a)) or of a semi-infinite slab (Fig. 1(b)) is a classical one in dielectric waveguide theory.

The mirror reflectivity is a crucial parameter of the laser, as it determines its oscillation condition. Moreover, dielectric slab antennas find applications at millimeter frequencies.

A variational formulation of the diffraction of TM waves by a semi-infinite slab was given in [1] as far back as 1957. In this treatment, the incident surface wave is used as a trial field. An analogous approach was used in [2] to discuss the diffraction of TE and TM waves, perpendicular to the p-n junction, at the mirror of a d.h. laser, as well as in [3].

A different approach based on a Fourier transform of the integral equation was introduced in [4]. An elegant approximate analysis neglecting mode conversion at the facet leads to an explicit expression of the far field, as elaborated in [5], whereas in [6] a theoretical comparison of various approximations is presented. A recent comprehensive review of the subject with numerous references can be found in [7], [8].

Steplike discontinuities in dielectric slabs (TE case) were analyzed in a previous paper [9]. There a higher order variational solution of the Ritz–Galerkin type was obtained by discretizing fields and Green's function by means of a sequence of appropriately scaled Laguerre functions. The above basic approach is the starting point of the present treatment.

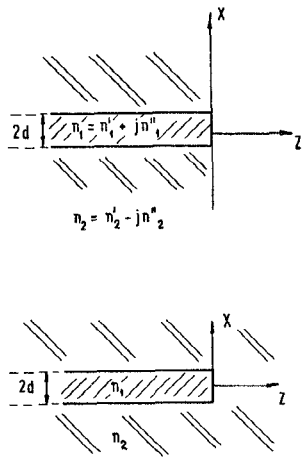

Fig. 1. Longitudinal cross section of laser, showing (a) facet with mirror, (b) facet with antireflection coating.

In the TE case, we can take advantage of the fact that as the effective frequency $vd = (n_1^2 - n_2^2)^{1/2} k_0 d$ goes to zero, the slab Green's function in the magnetic field formulation reduces to that of a homogeneous half-space. The latter is just the Hankel function whose exact representation in terms of the expanding functions of [9] can be obtained analytically. In this manner, the matrix elements of the total Green's function (air space and semi-infinite slab) are given by a closed expression plus a small correction $(0(vd)^2)$ to be determined numerically. This approach is analogous to the extraction of the quasi-static limit for discontinuity problems in closed waveguides. In the TM case, the above approach does not apply unless $n_1 \approx n_2$ as well.

The formulation of the TM problem in terms of the transverse electric field leads to an expression of the Green's function that is converging in the classical sense (unlike the magnetic field formulation). The transverse electric field is discontinuous at the dielectric interface however, an expansion in terms of continuous functions as in [9] is not suitable for large refractive index differences.

Manuscript received May 8, 1979.

T. E. Rozzi was with Philips Research Laboratories, Eindhoven, The Netherlands. He is now with the Department of Electrical Engineering and Electronics, University of Liverpool, P. O. Box 147, Liverpool, L69 3BX, England.

G. H. in't Veld is with Philips Research Laboratories, Eindhoven, The Netherlands.

0018-9480/80/0200-0061$00.75 ©1980 IEEE

This difficulty is avoided by employing two separate sequences of expanding functions: one inside the slab, the other outside it.

The above analysis applies to other TE and TM discontinuity problems, such as in [10] for instance.

In the examples, the effect of coupling between surface modes at the mirror of a LOC laser is investigated in detail and found to be insignificant. The effect of an antireflection coating at the mirror is to reduce the laser configuration of Fig. 1(a) to that of the semi-infinite slab of Fig. 1(b). Scattering properties and near fields in the two configurations are compared.

The effect of gain in the active region and loss outside is taken into account. This is not significant in the direction perpendicular to the p-n junction, whereas it provides the very guiding mechanism parallel to it. In fact, an exact treatment of the mirror reflectivity of the laser would involve solving the three-dimensional diffraction problem of a semi-infinite guide with a sharp dielectric boundary in the direction perpendicular to the junction and a diffused one parallel to it. Gain-induced parallel modes, however, can be reasonably well simulated by the modes of an active dielectric slab in a lossy medium, particularly for configurations with transverse current confinement. Excluding some special configuration such as buried heterostructures, the stripewidth (3–10 μm) is considerably larger than the thickness of the active layer (0.3 μm). Hence, it is reasonable to break down the hybrid mode problem [11] (resulting from the two-dimensional cross section) into a perpendicular TE-mode problem and a parallel TM one to be solved successively by means of the Effective Dielectric Constant procedure [12]. If required, the total reflectivity could then be deduced by combining the two reflectivities in a manner analogous to that discussed in [7], [13] on a spectral basis.

The variation of the reflection coefficient of the parallel mode and of the near and far fields with varying gain and stripewidth are numerically investigated.

II. Waveguide Modes

The basic configuration under study is depicted in Fig. 1. It consists of a dielectric slab of width $2d$ and complex refractive index $n_1 = n_1' + jn_1''$ enclosed between two semi-infinite layers of complex refractive index $n_2 = n_2' - jn_2''$, $(n_2' < n_1')$. The structure is terminated abruptly at $z = 0$. Owing to symmetry, we need only consider $x \geq 0$. As a consequence of the discontinuity at $z = 0$, the incoming surface wave couples to the continuous spectrum of the slab and of the air half-space ($z > 0$).

A. Surface Wave

1) TM: The transverse field component of a surface wave mode of the slab H_y and E_x is given by

$$E_x(x) = \frac{1}{\epsilon(x)} u(x) \tag{1a}$$

$$H_y(x) = \frac{\omega \epsilon_0}{\beta} u(x) \equiv Y_0 u(x) \tag{1b}$$

where

$$\epsilon(x) = \begin{cases} n_1^2, & x < d \\ n_2^2, & x > d. \end{cases}$$

β is the propagation constant of the surface wave. $u(x)$, which is proportional to the x-component of the electrical displacement vector, for even modes is given by

$$u(x) = \begin{cases} a \cos \kappa x, & x \leq d \qquad (2a) \\ a \cos \kappa d e^{-\gamma(x-d)}, & x \geq d. \qquad (2b) \end{cases}$$

The wavenumbers κ and γ are related by the conservation equation

$$\kappa^2 + \gamma^2 = (n_1^2 - n_2^2) k_0^2 \equiv v^2 \tag{3a}$$

and the dispersion relation

$$\kappa \tan \kappa d = (n_1/n_2)^2 \gamma. \tag{3b}$$

The normalization constant a in (2) is fixed by the requirement

$$\int_0^\infty \frac{1}{\epsilon(x)} u^2(x) dx = 1 \tag{4}$$

to be

$$a = n_1 \left[\frac{2}{d + (n_1 n_2)^2 (\kappa + \gamma^2)/(n_2^4 \kappa + n_1^4 \gamma)/\gamma} \right]^{1/2}. \tag{5}$$

The odd modes are determined by interchanging sin and cos in (2) and setting $\kappa d \to \kappa d + \pi/2$ in (3).

2) TE: In the TE case the relevant transverse field components are H_x and E_y given by

$$E_y(x) = u(x) \tag{6}$$

$$-H_x(x) = \frac{\beta}{\omega \mu_0} u(x) = Y_0 u(x). \tag{7}$$

$u(x)$ is given by 2. The conservation equation is the same as (3a). The dispersion relation is

$$\kappa \tan \kappa d = \gamma. \tag{8}$$

The normalization is such that

$$\int_0^\infty u^2(x) dx = 1 \tag{9}$$

and consequently

$$a = \sqrt{\frac{2}{d + 1/\gamma}}. \tag{10}$$

B. Continuous Spectrum

1) TM: The H_y component of a mode of the continuous spectrum of the region $z < 0$, for even modes, is given by

$$H_y(x, \mu) = Y(\mu) \phi(x, \mu) \tag{11}$$

with

$$\phi(x, \mu) = \begin{cases} \sqrt{\frac{2}{\pi}} \frac{n_2}{C} \cos sx, & x \leq d \\ \sqrt{\frac{2}{\pi}} n_2 \cos[s(x-d) + \alpha], & x \geq d \end{cases} \tag{12a, 12b}$$

where

$$Y(\mu)=\begin{cases}\dfrac{\omega\epsilon_0}{\sqrt{n_2^2k_0^2-\mu^2}}=\dfrac{\omega\epsilon_0}{\beta(\mu)}, & n_2k_0>\mu\\ \dfrac{j\omega\epsilon_0}{\sqrt{\mu^2-n_2^2k_0^2}}, & n_2k_0<\mu\end{cases}\tag{13}$$

$$s^2=\mu^2+v^2,\qquad 0\leqslant\mu<\infty\tag{14}$$

$$C=\left[\cos^2 sd+\left(\frac{n_2}{n_1}\right)^4\left(\frac{s}{\mu}\right)^2\sin^2 sd\right]^{1/2}\tag{15}$$

$$\alpha=\left[\tan^{-1}\frac{s}{\mu}\left(\frac{n_2}{n_1}\right)^2\tan sd\right],\qquad \left(\lim_{\mu\to\infty}\alpha=\mu d\right)\text{ and }n_1\to n_2.\tag{16}$$

The normalization condition is

$$\int_0^\infty\frac{dx}{\epsilon(x)}\phi(x,\mu)\phi(x,\mu')=\delta(\mu-\mu').\tag{17}$$

We can describe the field in the air region by means of a continuous spectrum of plane waves

$$\psi(x,\mu)=\sqrt{\frac{2}{\pi}}\cos\mu x\tag{18}$$

although a more compact representation (to be discussed later) will also be useful. The odd modes are obtained by replacing cos by sin in (12a), (18) and sd by $sd+\frac{\pi}{2}$ in (15), (16), and (12b).

2) TE: The even E_y and H_x components of the continuous spectrum are given by

$$E_y(x,\mu)=\phi(x,\mu)\tag{19}$$

$$-H_x(x,\mu)=Y(\mu)\cdot\phi(x,\mu)\tag{20}$$

where now

$$\phi(x,\mu)=\begin{cases}\sqrt{\dfrac{2}{\pi}}\ \dfrac{1}{C}\cos sx, & x\leqslant d\\ \sqrt{\dfrac{2}{\pi}}\ \cos[\,\mu(x-d)+\alpha], & x\geqslant d\end{cases}\tag{21}$$

$$Y(\mu)=\begin{cases}\sqrt{\dfrac{n_2^2k_0^2-\mu^2}{\omega\mu_0}}, & n_2k_-<\mu\\ \sqrt{\dfrac{\mu^2-n_2^2k_0^2}{j\omega\mu_0}}, & n_2k_0<\mu\end{cases}\tag{22}$$

$$\alpha=\tan^{-1}\left(\frac{s}{\mu}\tan sd\right)\qquad\left(\lim_{\mu\to\infty}\alpha=\mu d\right)\tag{23}$$

$$C=\left[1+\frac{v^2}{\mu^2}\sin^2 sd\right]^{1/2}\tag{24}$$

and

$$\int_0^\infty\phi(x,\mu)\phi(x,\mu')dx=\delta(\mu-\mu').\tag{25}$$

It is worthwhile to observe that as $\mu^2\gg v^2$, we have

$$s\to\mu;\qquad\alpha\to\mu d,\quad C\to 1\tag{26}$$

and

$$\phi(x,\mu)\to\sqrt{\frac{2}{\pi}}\ \cos\mu x\tag{27}$$

i.e. the continuous spectrum of the slab reduces to the plane wave spectrum of a semi-finite homogeneous region. This is not the case for TM waves unless $n_1\approx n_2$ also.

III. Integral Equation Formulation and Green Function: TM Case

Consider n surface waves to be propagating in the slab, characterized by the functions $u_1\cdots u_n$. Let the electric field amplitudes of the incoming and reflected waves at $z=0$ be expressed by the vectors $\boldsymbol{A}$ and $\boldsymbol{B}$, respectively. Let $b(\mu)$ denote the amplitude of the scattered modes of the continuous spectrum in the slab and $d(\mu)$ that in air. Continuity of E_x at $z=0$ requires

$$E_x(x)=\sum_{k=1}^n(A_k+B_k)\frac{u_k(x)}{\epsilon(x)}+\int_0^\infty b(\mu)\frac{\phi(x,\mu)}{\epsilon(x)}d\mu=\int_0^\infty d(\mu)\psi(x,\mu)d\mu\tag{28}$$

while continuity of H_y requires

$$H_y(x)=\sum_{k=1}^n Y_{0k}(A_k-B_k)u_k(x)-\int_0^\infty Y(\mu)b(\mu)\phi(x,\mu)d\mu=\int_0^\infty Y_0(\mu)d(\mu)\psi(x,\mu)d\mu\tag{29}$$

where

$$Y_0(\mu)=\begin{cases}\dfrac{\omega\epsilon_0}{\sqrt{k_0^2-\mu^2}}, & k_0>\mu\\ \dfrac{j\omega\epsilon_0}{\sqrt{\mu^2-k_0^2}}, & k_0<\mu.\end{cases}\tag{30}$$

B_k, $b(\mu)$, and $d(\mu)$ can be obtained by orthogonality from (28). Hence, the integral equation for the electric field is

$$\sum_{k=1}^n Y_{0k}A_ku_k(x)=\int_0^\infty Y(x,x')E_x(x')dx'\tag{31}$$

where

$$2Y(x,x')=\sum_{k=1}^n Y_{0k}u_k(x)u_k(x')+\int_0^\infty[\,Y(\mu)\phi(x,\mu)\phi(x',\mu)+Y_0(\mu)\psi(x,\mu)\psi(x',\mu)\,]d\mu.\tag{32}$$

Let E_l be the solutions of (31) with $A_l=1$; $A_{k\neq l}=0$. The scattering matrix of the discontinuity, as seen by the surface waves of the slab is then

$$S_{kl}=-\delta_{kl}+\int_0^\infty E_lu_k\,dx.\tag{33}$$

We observe that $E_x(x)$ is discontinuous at $x=d$, namely

$$n_1^2E_x(d^-)=n_2^2E_x(d^+).\tag{34}$$

Instead of using (28) in (29), obtaining an *electric* field description, it is equally possible to proceed the other way

round, obtaining a *magnetic* field description. This is given in Appendix III.

IV. Discrete Representation and Ritz–Galerkin Solution: TM Case

The integral equation (31) is amenable to a Ritz–Galerkin variational solution with good convergence properties if account is taken of the discontinuous jump of E_x at $x=d$. Using a complete expanding set continuous over the interval $0\leqslant x<\infty$ as for the TE case [9] is less satisfactory here unless $n_1\approx n_2$, for more terms would be required. We shall introduce instead a piecewise continuous expansion. The E_x component of the surface wave $u(x)/\epsilon(x)$ can be written as a two-component vector

$$\frac{u(x)}{\epsilon(x)}=a\begin{pmatrix}(1/n_1^2)\cos\kappa x\\(1/n_2^2)\cos\kappa d e^{-\gamma(x-d)}\end{pmatrix}\equiv\begin{pmatrix}(1/n_1^2)u_1(x)\\(1/n_2^2)u_2(x)\end{pmatrix} \tag{35}$$

where the first component represents the field in the interval $0\leqslant x<d$ and the second in the interval $d<x$.

A similar description applies to the E_x component of a mode of the continuous spectrum. Consider now a function $f(x)$, continuous over each subinterval, where it takes the form $f_1(x)$ and $f_2(x)$, respectively, but possibly discontinuous at $x=d$. The "scalar" product in functional sense of $u(x)/\epsilon(x)$ is just

$$\left\langle\frac{u}{\epsilon},f\right\rangle=\int_0^\infty\frac{u(x)}{\epsilon(x)}f(x)dx$$
$$=\frac{1}{n_1^2}\int_0^d u_1(x)f_1(x)+\frac{1}{n_2^2}\int_d^\infty u_2(x)f_2(x)dx. \tag{36}$$

In each interval, we can find a separate discrete sequence of expanding functions

$$c_m(x):0\leqslant x\leqslant d,\qquad m=0,1,\cdots,M$$
$$\mathcal{L}_n(x-d):d\leqslant x,\qquad n=0,1,\cdots,N. \tag{37}$$

The c_m's are complete in the limit $M\to\infty$ and possibly orthonormal over the interval of definition and so are the $\mathcal{L}_n$'s. By means of the set (37), the function $u(x)/\epsilon(x)$ is transformed into the $M+N+2$-dimensional vector

$$\tilde{Q}=\begin{bmatrix}(1/n_1^2)Q_1\\\hline(1/n_2^2)Q_2\end{bmatrix}\begin{matrix}\}\ M+1\\\}\ N+1\end{matrix} \tag{38}$$

where

$$u_1(x)=\sum_{m=0}^{M}Q_{1m}c_m(x) \tag{39a}$$

$$u_2(x)=\sum_{n=0}^{N}Q_{2n}L_n(x-d). \tag{39b}$$

If a similar expansion holds for the arbitrary function $f(x)$ so that $f\to(F_1F_2)$, then the "scalar product" (36) reduces to the ordinary scalar product of two $M+N+2$-dimensional vectors:

$$\left\langle\frac{u}{\epsilon},f\right\rangle=\left(\frac{1}{n_1^2}Q_1^T,\frac{1}{n_2^2}Q_2^T\right)\cdot\begin{pmatrix}F_1\\F_2\end{pmatrix}. \tag{40}$$

In view of the behavior of the surface wave mode, an appropriate choice of the "basis" (37) is

$$c_m(x)=\sqrt{\frac{2\epsilon_m}{d}}\cos\frac{m\pi x}{d} \tag{41}$$

with

$$\epsilon_m=\begin{cases}\frac{1}{2}, & m=0\\1, & m>0\end{cases}$$
$$\int_0^d c_m(x)c_n(x)dx=\delta_{mn} \tag{42}$$

and

$$\mathcal{L}_n(x-d)=\frac{1}{\sqrt{x_0}}L_n\left(\frac{x-d}{x_0}\right)e^{-(x-d)/2x_0} \tag{43}$$

$$\int_d^\infty\mathcal{L}_m(x-d)\mathcal{L}_n(x-d)=\delta_{mn}. \tag{44}$$

The L_n's are the ordinary Laguerre polynomials, x_0 is a scale factor to be determined so as to "optimize" the finite expansion. A useful criterion is to minimize the error of the representation of the incident mode outside the core. If γ is real, the representation is trivially simple: we just set $N=0$, $x_0=\dfrac{1}{2\gamma}$.

As γ is complex in general, we use a minimum square approximation for any given N. Another criterion consists of imposing the continuity of u at $x=d$, i.e., from (41) and (43)

$$\sum_{n=0}^{M}Q_{1m}\cdot\sqrt{\frac{2\epsilon m}{d}}\cdot(-1)^m=\sum_{n=0}^{N}\frac{Q_{2n}(x_0)}{\sqrt{x_0}}. \tag{45}$$

The former is suited to describe the "tail" of the field, but does not ensure *a priori* that the condition at the interface $x=d$ is satisfied. The contrary holds for the latter. The coefficients of the expansion (39) are found by straightforward integration

$$Q_{1m}=a\begin{cases}\sqrt{2\epsilon_m d}\,(-)^m\dfrac{\sin\kappa d\cdot\kappa d}{(\kappa d)^2-(m\pi)^2}, & \kappa d\neq m\pi\\[2ex]\sqrt{\dfrac{\epsilon_m d}{2}}, & \kappa d=m\pi\end{cases} \tag{46}$$

and

$$Q_{2n}=a\sqrt{x_0}\cos\kappa d\left(\gamma x_0-\tfrac{1}{2}\right)^n\left(\gamma x_0+\tfrac{1}{2}\right)^{-n-1}.$$

A formally similar expansion (but convergent only in distributional sense) holds for the modes of the continuous spectrum

$$\phi(x,\mu)\to P=\begin{bmatrix}P_1(\mu)\\P_2(\mu)\end{bmatrix} \tag{47}$$

where

$$P_{1m}=\begin{cases}\dfrac{2}{C}\sqrt{\dfrac{\epsilon_m d}{\pi}}\,(-1)^m\dfrac{\sin sd\cdot sd}{(sd)^2-(m\pi)^2}, & sd\neq m\pi\\[2ex]\dfrac{1}{C}\sqrt{\dfrac{\epsilon_m d}{\pi}}, & sd=m\pi\end{cases} \tag{48a}$$

and [9, appendix I]

$$P_{2n}=\sqrt{\frac{2x_0}{\pi}}\ \frac{(-1)^n}{\left(\frac{1}{4}+\mu^2x_0^2\right)^{1/2}}\cos\left[(2n+1)\tan^{-1}2\mu x_0+\alpha\right]. \tag{48b}$$

The expansion for the continuous spectrum in the air half-space is

$$\psi(x,\mu)\to\boldsymbol{P}^0=\begin{pmatrix}\boldsymbol{P}_1^0\\ \boldsymbol{P}_2^0\end{pmatrix}$$

with

$$P_{1m}^0=\begin{cases}2\sqrt{\frac{\epsilon_m d}{\pi}}\ (-1)^m\frac{\sin\mu d\cdot\mu d}{(\mu d)^2-(m\pi)^2}, & \mu d\neq m\pi\\ \sqrt{\frac{\epsilon_m d}{\pi}}\ , & \mu d=m\pi\end{cases} \tag{49}$$

$$P_{2m}^0=\sqrt{\frac{2x_0}{\pi}}\ \frac{(-1)^n}{\left(\frac{1}{4}+\mu^2x_0^2\right)^{1/2}}\cos\left[(2n+1)\tan^{-1}2\mu x_0+\mu d\right]. \tag{50}$$

The terms of the above sequences of expanding functions E_x is expressed as the (unknown) $M+N+2$-dimensional vector

$$\tilde{\boldsymbol{F}}=\begin{bmatrix}(1/n_1^2)\boldsymbol{F}_1\\ \hline (1/n_2^2)\boldsymbol{F}_2\end{bmatrix} \tag{51}$$

and the integral equation (31) for the electric field with $A_l=1$; $A_{k\neq l}=0$ becomes the matrix equation

$$Y_{0l}\boldsymbol{Q}_l=\underline{\underline{\boldsymbol{Y}}}\cdot\tilde{\boldsymbol{F}}_l \tag{52}$$

where

$$\underline{\underline{\boldsymbol{Y}}}=\frac{\omega\epsilon_0}{2}\left\{\sum_{k-1}^{n}\frac{1}{\beta_k}\boldsymbol{Q}_k\boldsymbol{Q}_k^T+\int_0^\infty\left[\frac{1}{\sqrt{n_2^2k_0-\mu^2}}\boldsymbol{P}(\mu)\boldsymbol{P}^T(\mu)\right.\right.$$
$$\left.\left.+\frac{1}{\sqrt{k_0^2-\mu^2}}\boldsymbol{P}^0(\mu)\boldsymbol{P}^{0T}(\mu)\right]d\mu. \tag{53}$$

The normalized scattering matrix for the surface waves is

$$\bar{S}_{kl}=-\delta_{kl}+\sqrt{Y_{0k}Y_{0l}}\ \boldsymbol{Q}_k^T\cdot\bar{\boldsymbol{Y}}^{-1}\cdot\boldsymbol{Q}_l \tag{54}$$

while the scattering of a surface wave into a (radiative) mode of the continuous spectrum of either the slab or of the air region is

$$\bar{S}_{kl}=\pm(Y_{0k})^{1/2}\begin{Bmatrix}Y^{1/2}(\mu)\\ Y_0^{1/2}(\mu)\end{Bmatrix}\boldsymbol{Q}_k^T\cdot\bar{\boldsymbol{Y}}^{-1}\cdot\begin{Bmatrix}\boldsymbol{P}(\mu)\\ \boldsymbol{P}^0(\mu)\end{Bmatrix}. \tag{55}$$

The upper or the lower expressions are assumed according to whether the continuous mode belongs to the spectrum of the slab or of the air region, respectively.

V. Integral Equation and Green Function: TE Case

Unlike the TM case, in the TE case, both transverse components E_x and H_y are continuous across the dielectric interface. Two features result from this property.

i) The limit (26)–(27) holds for $\mu^2\gg v^2$, even if $n_1\gg n_2$.

ii) A continuous expanding set can be used.

The continuity equations for the TE case have already been discussed in [9]. The integral equations for the magnetic field with $A_l=1$, $A_{k\neq l}=0$ are

$$-Z_{0l}u_l(x)=\int_0^\infty dx'Z(x,x')h_l(x') \tag{56}$$

with the Green's function

$$Z(x,x')=\frac{\omega\mu_0}{2}\left\{\sum_{k=1}^{n}\frac{1}{\beta_k}u_k(x)u_k(x')\right.$$
$$+\int_0^\infty\frac{d\mu}{\sqrt{n_2^2k_0-\mu^2}}\phi(x,\mu)\phi(x',\mu)$$
$$\left.+\frac{2}{\pi}\int_0^\infty\frac{d\mu}{\sqrt{k_0^2-\mu^2}}\cos\mu x\cos\mu x'\right\}. \tag{57}$$

In the even case, the contribution of the air half-space region can be written compactly as

$$\frac{2}{\pi}\int_0^\infty\frac{d\mu}{\sqrt{k_0^2-\mu^2}}\cos\mu x\cos\mu x=\tfrac{1}{2}\sum_{\pm}H_0^{(2)}(k_0|x\pm x'|). \tag{58}$$

$H_0^{(2)}=J_0-jN_0$ is the Hankel function of the second type. No such close form expression is available for the contribution of the region $z<0$. However, it is convenient to extract the limit of lightly trapped waves $(vd)^2\ll1$) from the impedance of the latter region. In fact, we have

$$\int_0^\infty\frac{d\mu}{\sqrt{n_2^2k_0^2-\mu^2}}\phi(x,\mu)\phi(x',\mu)=\tfrac{1}{2}\sum_{\pm}H_0^{(2)}(n_2k_0|x\pm x'|)$$
$$+\int_0^\infty\frac{d\mu}{\sqrt{n_2^2k_0^2-\mu^2}}t(x,x';\mu). \tag{59}$$

The "difference" kernel

$$t(x,x';\mu)=\phi(x,\mu)\phi(x',\mu)-\frac{2}{\pi}\cos\mu x\cos\mu x' \tag{60}$$

is identically zero for $v=0$ and decreases as μ^{-3} for large μ. Hence, the total Green impedance function can be rewritten as

$$Z(x,x')=\frac{\omega\mu_0}{2}\left\{\sum_{k=1}^{n}\frac{1}{\beta_k}u_k(x)u_k(x')\right.$$
$$+\tfrac{1}{2}\left[\sum_{\pm}H_0^{(2)}(k_0|x\pm x'|)\right.$$
$$\left.\left.+H_0^{(2)}(n_2k_0|x\pm x'|)\right]\right.$$
$$\left.+\int_0^\infty\frac{1}{\beta(\mu)}t(x,x';\mu)d\mu\right\}. \tag{61}$$

Analogous results hold for the odd case. The electric field formulation is given in Appendix IV. Owing to feature ii) mentioned above, the normalized Laguerre functions (43) can be employed as expanding functions over the whole interval $0 \leqslant x \leqslant \infty$. The functions $u(x)$, $\phi(x,\mu)$ are mapped into the $N+1$-dimensional vectors $\boldsymbol{Q}_k$ and $\boldsymbol{P}(\mu)$, respectively. These have been derived in [9] and are reported in Appendix I for ease of reference. The advantage of introducing the Hankel function in the preceding formulation is that the matrix elements

$$H_{mn}(\gamma)=\tfrac{1}{2}\int_0^\infty\int_0^\infty dxdx' L_m(x) \cdot\left[H_0^{(2)}(\gamma|x+x'|)+H_0^{(2)}(\gamma|x-x'|)\right]L_n(x') \quad (62)$$

can be derived *analytically*. Derivation and result are given in Appendix II. Hence, the integral equation for the *magnetic* field formulation becomes the matrix equation

$$Z_{0l}\boldsymbol{Q}_l=\underline{\underline{\boldsymbol{Z}}}\cdot\boldsymbol{G}_l. \quad (63)$$

$\boldsymbol{G}_l$ corresponds to the unknown $h_l(x)$ and

$$\underline{\underline{\boldsymbol{Z}}}=\frac{\omega\mu_0}{2}\sum_k\frac{1}{\beta_k}\boldsymbol{Q}_k\boldsymbol{Q}_k^T+\bar{\boldsymbol{H}}(k_0)+\bar{\boldsymbol{H}}(n_2k_0) +\int_0^\infty\frac{d\mu}{\sqrt{n_2^2k_0^2-\mu^2}}\left[\boldsymbol{P}(\mu)\boldsymbol{P}^T(\mu)-\boldsymbol{P}^0(\mu)\boldsymbol{P}^{0T}(\mu)\right]. \quad (64)$$

The scattering matrix between surface waves is given by

$$\bar{S}_{kl}=\delta_{kl}-\sqrt{Z_{0k}Z_{0l}}\;\boldsymbol{Q}_k^T\cdot\underline{\underline{\boldsymbol{Z}}}^{-1}\cdot\boldsymbol{Q}_l \quad (65)$$

while the coupling between surface waves and the continuous spectrum is given by

$$\bar{S}_k(\mu)=\mp Z_{0k}^{1/2}\begin{Bmatrix}Z^{1/2}(\mu)\\ Z_0^{1/2}(\mu)\end{Bmatrix}\boldsymbol{Q}_k^T\cdot\underline{\underline{\boldsymbol{Z}}}^{-1}\cdot\begin{Bmatrix}\boldsymbol{P}(\mu)\\ \boldsymbol{P}^0(\mu)\end{Bmatrix} \quad (66)$$

the upper expression applying to continuous modes of the slab, the lower one to modes of the air region.

VI. Near and Far Field

A. TM Case

Once (52) has been solved, we obtain the approximate expansion of the near field as

$$E_x(x)=\begin{cases}\dfrac{1}{n_1^2}\displaystyle\sum_{m=0}^{M}F_{1m}c_m(x), & 0\leqslant x\leqslant d\\[2ex] \dfrac{1}{n_2^2}\displaystyle\sum_{n=0}^{N}F_{2m}\mathcal{L}_n(x-d), & d\leqslant x\end{cases} \quad (67)$$

The corresponding far field obtained by saddle point integration as in [9] is

$$H_y^R(r,\theta)/\omega\epsilon_0\approx\sqrt{\frac{1}{n\cdot k_0 r}}\;f(\theta)e^{-j(rnk_0-(\pi/4))} \quad (68)$$

where, in air, θ is measured from the positive z-axis, and we have $n=1$

$$f(\theta)=\left[\boldsymbol{P}_1^0(k_0\sin\theta),\boldsymbol{P}_2^0(k_0\sin\theta)\right]^T\cdot\tilde{\boldsymbol{F}}. \quad (69)$$

TABLE I
Convergence of Reflection Coefficient: TE_0 Mode*

N	$\lvert\Gamma\rvert$	$\angle\Gamma$ (degrees)
0	0.598	4.41
1	0.624	3.04
2	0.620	2.52
3	0.624	2.75
4	0.623	2.98
5	0.622	2.92
	With antireflection coating:	
4	0.024	0.18

*$d=0.3$ μm; $\lambda_0=0.9$ μm; $n_1\equiv n_1'=3.61$; $n_2\equiv n_2'=3.40$.

In the laser, θ is measured from the negative z-axis, $n=n_2$, and

$$f(\theta)=\left[\boldsymbol{P}_1^0(n_2k_0\sin\theta),\boldsymbol{P}_2^0(n_2k_0\sin\theta)\right]^T\cdot\tilde{\boldsymbol{F}} \cdot e^{-j[\alpha(\theta)-n_2k_0d\sin\theta]}. \quad (70)$$

B. TE Case

The near field is here given by

$$H_x(x)=\sum_{n=0}^{N}G_n\mathcal{L}_n(x) \quad (71)$$

while the far field is

$$E_y^R(r,\theta)/\omega\mu_0 =\begin{cases}\sqrt{\dfrac{1}{k_0r}}\;\boldsymbol{P}^{0T}(k_0\sin\theta)\cdot\boldsymbol{G}, & \text{in air}\\[2ex] \sqrt{\dfrac{1}{n_2k_0r}}\;\boldsymbol{P}^T(k_0\sin\theta)\cdot\boldsymbol{G}e^{-j[\alpha(\theta)-n_2k_0d\sin\theta]}, & \text{in the laser}\end{cases} \quad (72)$$

VII. Examples

The theory described in the previous sections will now be illustrated by means of a few examples.

A. Refractive Index Guiding

First, the convergence of the reflection coefficient of the TE_0 mode perpendicular to the junction for increasing order of the variational solution was tested for the standard configuration, perpendicular to the p-n junction, where

$$n_1=n_1'=3.61;\quad n_2=n_2'=3.40;\quad \lambda_0=0.9\ \mu m;\quad d=0.3\ \mu m.$$

The results are shown in Table I. The modulus of the reflection coefficient agrees quite well with that given in [2], [14] where the incident TE_0 mode is assumed as "trial field." This is to be expected, owing to the variational nature of the reflection coefficient. The near and far fields are compared in Fig. 2 with those resulting from assuming TE_0. In the latter, the near field is a real function, plotted as a broken line in Fig. 2(a). In the present treatment, the near field is a complex quantity, whose amplitude and phase are shown in Figs. 2(a), (b). In particular, there appears to be nonnegligible bending of the phase front just outside the active layer, where the flanks of the near field differ from those of the modal field. The correspond-

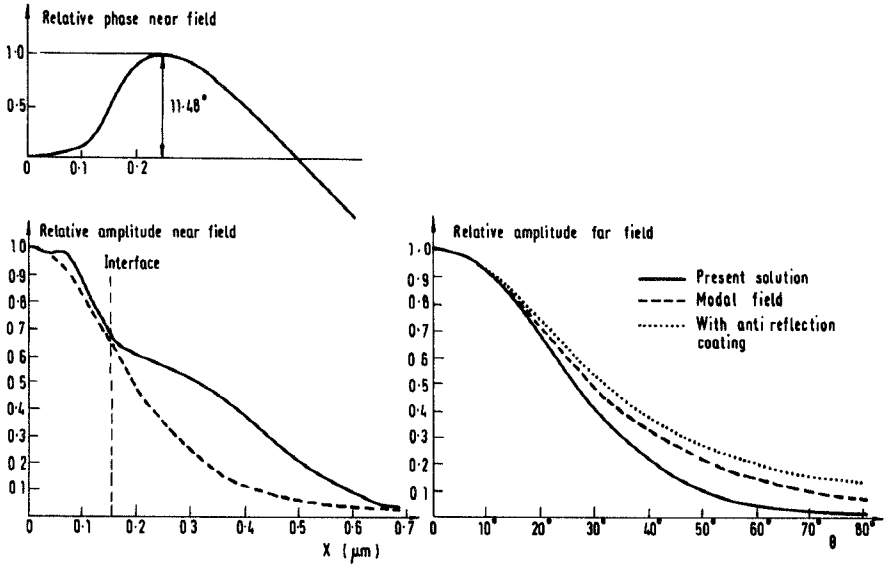

Fig. 2. Comparison of variational field (direction perpendicular to the junction) with modal field. (a) Amplitude of near field. (b) Phase of near field. (c) Amplitude of far field.

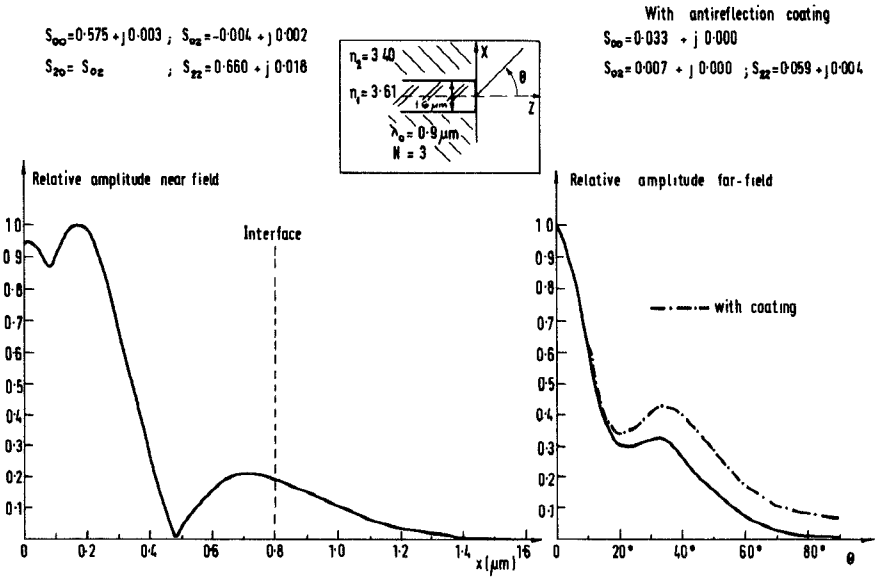

Fig. 3. Perpendicular field at the facet of Large Optical Cavity laser. Geometry shown in the insert. (a) Amplitude of near field. (b) Amplitude of far field.

ing far field is compared in Fig. 2(c) with that obtained from the modal field by means of a Fourier transform, including the correction for the "obliquity factor" [14], [15] and seem to agree even better with the experimental results of [16]. The inclusion of gain in the thin layer, typically 50 200 cm^{-1}, and of free-carrier loss (5 cm^{-1}) in the surrounding region does not appreciably alter these results, except for a very slight narrowing of the near field.

The question arose whether in a large optical cavity laser, where possibly more than one E^x mode can propagate, significant modal coupling can take place at the mirror. Typical results are shown in Fig. 3. TE_0 and TE_2 are propagating and TE_0 is incident. Mode coupling as given by $|S_{02}|$ is insignificant. The magnitudes of the reflection coefficients $|S_{00}|$ and $|S_{22}|$ agree quite well with the values found in [2]. However, the near field plotted in Fig. 3(a) differs from that of the incident TE_0 mode. The corresponding far field is given in Fig. 3(b).

B. Antireflection Coating

Placing an antireflection coating on the laser mirror reduces the configuration of Fig. 1(a) to that of a semi-infinite slab radiating into a half-space n_2 shown in Fig. 1(b). The ensuing reduction of the reflection coefficient is shown in Table I for $d=0.3$ μm. The near field is now fairly close to that of the incident TE_0 mode. The ampli-

tude of the far field (Fig. 2(c) for the standard configuration $d=0.3$ μm and Fig. 3(b) for the LOC case $d=1.6$ μm) shows a somewhat broader radiation pattern.

C. Gain Guiding

Fig. 4 gives a somewhat idealized picture of the laser cross section, neglecting diffusion parallel to the junction. In this direction mode confinement (guiding) is provided by gain g in the GaAs region under the stripe (active region) and by loss outside it. The above two-dimensional cross section is replaced by the slab configuration of Fig. 4(b) by means of the effective dielectric constant procedure. If we assume a hybrid E^x mode (TE perpendicular to the junction), we must then consider a TM mode parallel to it.

As mentioned in Section III, the E_x-component is slightly discontinuous of the interface so that $(\epsilon E_x)_{w/2}- = (\epsilon E_x)_{w/2}+$. This condition is not satisfied *a priori* by the variational solution since the expansion inside and outside the stripe are independent and converge separately in the mean. The convergence of the variational solution, for a 5-μm wide stripe with a gain of 300 cm^{-1} in the active region, is shown in Fig. 5. The near and far fields for $M=0,1,4$, $N=0,4$ are compared with those obtained, assuming the incident modal field as near field and its Fourier transform as far field.

The amplitude of the modal field and the variational near field are virtually identical under the stripe and differ somewhat in the tail outside it. Taking $M=1$, $N=0$, i.e. a two-term Fourier cosine expansion with complex coefficients under the stripe and a single exponential term outside is quite satisfactory in all respects. The phase of the near field, albeit significant, does not differ appreciably from that of the incident (complex) mode and, as such, is not plotted. The magnitude of the far field is hardly sensitive to the details of the near field; so assuming the latter to be the incident modal field gives virtually identical results. The variation of the reflection coefficient with gain and stripewidth in the region $3 \leqslant w \leqslant 6$ μm was also investigated and found to be rather minor.

D. Gain Guiding and Refractive Index Antiguiding

Owing to the relationship between real and imaginary part of the refractive index, gain guiding is necessarily accompanied by refractive index antiguiding. The ratio between the latter and the former is estimated to be in the region of 0.5–3 by various authors [17], [18]. We assume the lower value in considering the configuration of the insert of Fig. 6.

Plotted are the far fields for $w=3$, 5 μm and for three different values of the gain. It is interesting to note the appearance of sidelobes for the smaller stripe and lower gain values. These lobes become more prominent with increasing antiguiding. Also, for the smaller stripewidth, the influence of the gain on the field pattern and on the reflection coefficient is somewhat more marked, as to be expected.

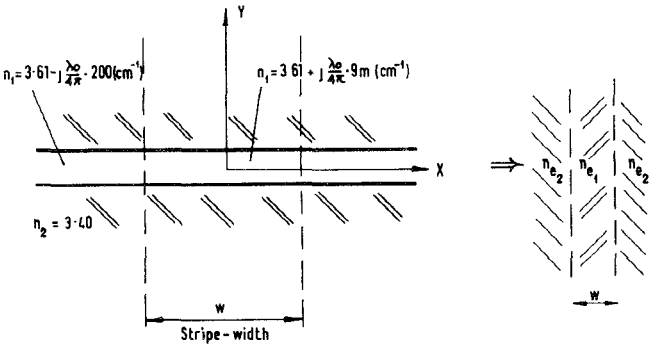

Fig. 4. Idealized geometry for computing fields parallel to the junction. (a) Original two-dimensional cross section. (b) Equivalent one-dimensional cross section after application of the Effective Dielectric Constant procedure.

VIII. Conclusions

We have derived a rigorous variational treatment of the abrupt discontinuity at the end plane of a dielectric (active or lossy) slab in a lossy medium under the assumption of small aspect ratio.

New theoretical results allow the discretization of the Green's functions for both TE and TM cases in both electric and magnetic field formulations. Numerical results are provided for the d.h. laser configuration. From these, it appears that assuming the incident field as trial field gives an accurate estimate of the modulus of the reflection coefficient in both directions, parallel and perpendicular to the junction as expected, as well as a good guess of the near field parallel to the junction. Significant differences, however, arise in the near and far fields perpendicular to the junction. In particular, the amplitude of the far field decreases faster than previously theoretically predicted, even including the "obliquity factor" correction. Correspondingly, the phase of the above near field presents a significant distortion previously unreported.

The analytical techniques presented are quite general and can be applied to various types of dielectric discontinuities at optical and microwave frequencies.

Appendix I

Components of the Vectors Appearing in Section V (TE Case)

$$Q_{kn} = a\sqrt{x_0}\left\{(-1)^n \frac{\cos\left[(2n+1)\tan^{-1}2kx_0\right]}{\left[\frac{1}{4}+(kx_0)^2\right]^{1/2}} + \sum_{k=0}^{n}(-1)^k L_{n-k}^{k}\left(\frac{d}{x_0}\right) \cdot \left[\frac{\cos kd}{\left(\frac{1}{2}+\gamma x_0\right)^{k+1}} + \frac{\cos\left[(k+1)\tan^{-1}2kx_0 + kd\right]}{\left[\frac{1}{4}+(kx_0)^2\right]^{1/2}}\right]\right\},$$

$$\cdot n = 0,1 \ldots N. \quad \text{(A.1)}$$

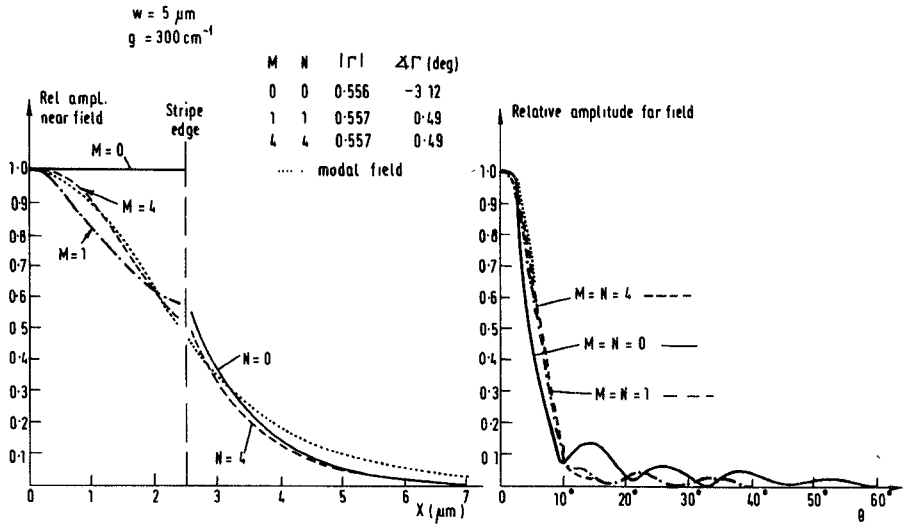

Fig. 5. Convergence of the variational solution in the direction parallel to the junction. Gain guiding. (a) Amplitude of near field. (b) Amplitude of far field.

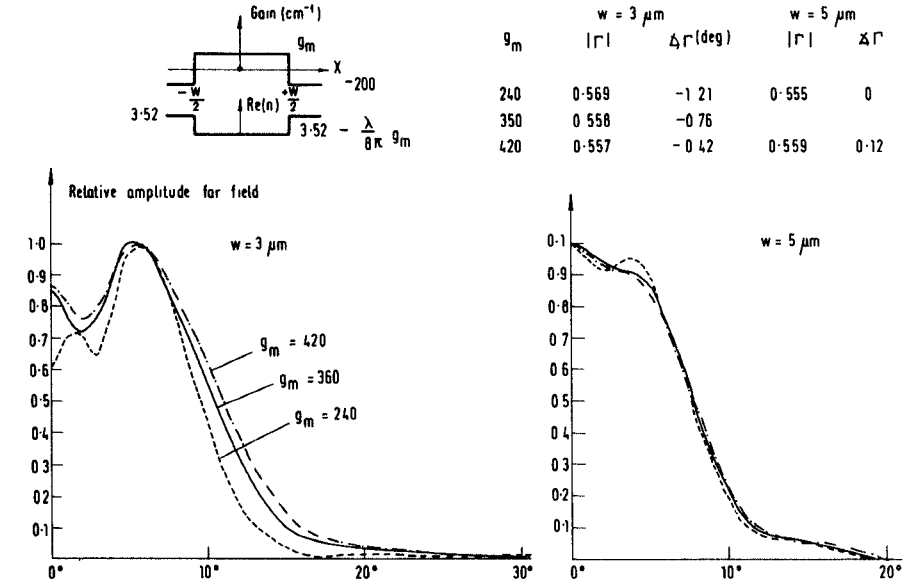

Fig. 6. Amplitude of the far field (direction parallel to the junction) for different values of gain and stripewidth. Gain guiding and refractive index antiguiding.

$$P_n(\mu)=\sqrt{\frac{2x_0}{\pi}}\left\{\frac{(-1)^n}{C}\frac{\cos\left[(2n+1)\tan^{-1}2sx_0\right]}{\left[\frac{1}{4}+(sx_0)^2\right]^{1/2}}\right.$$

$$+\sum_{k=0}^{n}(-1)^k e^{-d/2x_0}L_{n-k}^{k}\left(\frac{d}{x_0}\right)\left[\frac{\cos\left[(k+1)\tan^{-1}2\mu x_0+\alpha\right]}{\left[\frac{1}{4}+(\mu x_0)^{2(k+1)/2}\right]}\right.$$

$$\left.\left.-\frac{1}{C}\frac{\cos\left[(k+1)\tan^{-1}2sx_0+sd\right]}{\left[\frac{1}{4}+(sx_0)^2\right]^{(k+1)/2}}\right]\right\}. \tag{A.2}$$

Appendix II

It is required to compute

$$H_{pq}^{\mp}(k_0)=\int_0^\infty e^{-x/2x_0}L_p\left(\frac{x}{x_0}\right)\frac{dx}{\sqrt{x_0}}\int_0^\infty e^{-x/2x_0}L_q\left(\frac{x'}{x_0}\right)$$
$$\cdot H_0^{(2)}(k_0|x\mp x'|)\frac{dx'}{\sqrt{x_0}}. \tag{A.3}$$

Let us introduce the expansion

$$H_0(k_0|x-x'|)=\frac{e^{-|x-x'|/2x_0}}{x_0}\sum_{k=0}^{\infty}a_k L_k\frac{|x-x'|}{x_0} \tag{A.4}$$

with coefficients to be determined later. Using (A.4) in

(A.3) we obtain

$$H_{pq}^{-}=\sum_{k=0} a_k I_k$$

with

$$\begin{aligned}I_k&=\int_0^\infty e^{-x/2x_0}L_p\left(\frac{x}{x_0}\right)\frac{dx}{x_0}\int_0^\infty \frac{dx'}{x_0}e^{-x'/2x_0}L_q\left(\frac{x'}{x_0}\right)\\&\quad\cdot e^{-|x-x'|/2x_0}L_k\left(\frac{|x-x'|}{x_0}\right)\\&=\int_0^\infty e^{-x/x_0}L_p\left(\frac{x}{x_0}\right)\frac{dx}{x_0}\int_0^x L_q\left(\frac{x'}{x_0}\right)L_k\left(\frac{x-x'}{x_0}\right)\frac{dx'}{x_0}\\&\quad+\int_0^\infty L_p\left(\frac{x}{x_0}\right)\frac{dx}{x_0}\int_x^\infty e^{-x'/x_0}L_q\left(\frac{x'}{x_0}\right)L_k\left(\frac{x'-x}{x_0}\right)\frac{dx'}{x_0}\\&\equiv I_k'+I_k''.\end{aligned}\tag{A.5}$$

Hence, setting $\frac{x-x'}{x_0}=u$, we have

$$\begin{aligned}I_k'&=\int_0^\infty e^{-x/x_0}L_p\left(\frac{x}{x_0}\right)\frac{dx}{x_0}\int_0^{x/x_0}L_k(u)L_q\left(\frac{x}{x_0}-u\right)du\\&=\int_0^\infty e^{-x/x_0}L_p\left(\frac{x}{x_0}\right)\frac{dx}{x_0}\left[L_{k+q}\left(\frac{x}{x_0}\right)-L_{k+q+1}\left(\frac{x}{x_0}\right)\right]\\&=\delta_{p,k+q}-\delta_{p,k+q+1}.\end{aligned}\tag{A.6}$$

Similarly, setting $\frac{x'-x}{x_0}=u$ in the second integral in (A.5) we have

$$I_k''=\int_0^\infty \frac{dx}{x_0}L_p\left(\frac{x}{x_0}\right)e^{-x/x_0}\int_0^\infty e^{-u}L_k(u)L_q\left(u+\frac{x}{x_0}\right)du.\tag{A.7}$$

However, using integration by parts, we obtain

$$\begin{aligned}\int_0^\infty e^{-u}L_k(u)L_q\left(u+\frac{x}{x_0}\right)du&=\int_0^\infty L_q\left(u+\frac{x}{x_0}\right)d\\&\quad\cdot\left\{e^{-u}\left[L_{k-1}(u)-L_k(u)\right]\right\}\\&=\int_0^\infty L_{q-1}^1\left(u+\frac{x}{x_0}\right)e^{-u}\left[L_{k-1}(u)-L_k(u)\right].\end{aligned}\tag{A.8}$$

Using the result [19, p. 1038]

$$L_{q-1}^1\left(u+\frac{x}{x_0}\right)=\sum_{m=0}^{q-1}L_m(u)L_{q-1-m}\left(\frac{x}{x_0}\right)\tag{A.9}$$

(A.8) can be rewritten as

$$\begin{aligned}&\sum_{m=0}^{q-1}L_{q-1-m}\left(\frac{x}{x_0}\right)\int_0^\infty e^{-u}\left[L_{k-1}(u)-L_k(u)\right]L_m(u)du\\&\qquad=\sum_{m=0}^{q-1}L_{q-1-m}\left(\frac{x}{x_0}\right)\left[\delta_{m,k-1}-\delta_{m,k}\right]\\&\qquad=L_{q-k}\left(\frac{x}{x_0}\right)-L_{q-1-k}\left(\frac{x}{x_0}\right).\end{aligned}\tag{A.10}$$

Hence

$$I_k''=\delta_{p,q-k}-\delta_{p,q-1-k}\tag{A.11}$$

which, together with (A.6), gives

$$H_{pq}^{-}=a_{p-q}-a_{p-q-1}+a_{q-p}-a_{q-1-p}\tag{A.12}$$

($a_k=0$ for $k<0$). In order to compute H^+, let us again use (A.4) with the minus sign changed into plus. Using (A.29–35), we get

$$\begin{aligned}H_{pq}^{+}&=\sum_k a_k\int_0^\infty e^{-x/x_0}L_p\left(\frac{x}{x_0}\right)\frac{dx}{x_0}\\&\quad\cdot\int_0^\infty e^{-x'/x_0}L_q\left(\frac{x'}{x_0}\right)e^{-|x-x'|/2x_0}L_k\left(\frac{x+x'}{x_0}\right)\frac{dx'}{x_0}\\&=a_{p+q}-a_{p+q+1}.\end{aligned}\tag{A.13}$$

Hence the result

$$\begin{aligned}H_{pq}(k_0)&\equiv H_{pq}^{+}(k_0)+H_{pq}^{-}(k_0)\\&\equiv\tfrac{1}{2}(a_{p+q}-a_{p+q+1})\\&\quad+\tfrac{1}{2}(a_{p-q}-a_{p-q-1}+a_{q-p}-a_{q-p-1}).\end{aligned}\tag{A.14}$$

It still remains the task of evaluating the coefficients of the expansion (A.6)

$$a_k=x_0\int_0^\infty e^{-u/2}H_0^{(2)}(k_0x_0u)L_k(u)du.$$

Using the expansion of the Laguerre polynomials [19, p. 1037] we obtain

$$\begin{aligned}a_k&=x_0\sum_{m=0}^{k}(-1)^m\binom{k}{k-m}\frac{1}{m!}\left[\int_0^\infty e^{-u/2}H_0^{(2)}(k_0x_0u)u^m du\right]\\&=x_0\sum_{m=0}^{k}(-1)^m\binom{k}{k-m}\left(\tfrac{1}{4}+k_0^2x_0^2\right)^{-1/2(m+1)}\\&\quad\cdot\left\{P_m\left[\left(1+4k_0^2x_0^2\right)^{-1/2}\right]+j\frac{2}{\pi}Q_m\left[\left(1+4k_0^2x_0^2\right)^{-1/2}\right]\right\}\end{aligned}\tag{A.15}$$

where the definition of the Hankel function $H_0^{(2)}=J_0-jN_0$ and [19, pp. 7–11] have been used. P and Q are the Legendre polynomials of order m. Let

$$\phi_0=\arctan 2k_0x_0\tag{A.16}$$

$$\cos\phi_0=\left(1+4k_0^2x_0^2\right)^{-1/2}.\tag{A.17}$$

Hence

$$\begin{aligned}a_k(k_0)&=x_0\sum_{m=0}^{k}(-1)^m\binom{k}{k-m}(2\cos\phi_0)^{m+1}\\&\quad\cdot\left[P_m(\cos\phi_0)+j\frac{2}{\pi}Q_m(\cos\phi_0)\right],\qquad k\geqslant 0\\&=0,\qquad k<0.\end{aligned}\tag{A.18}$$

Appendix III

Magnetic Field Formulation: TM Modes

From (28) and (29) by orthogonality, we obtain the

integral equation for H_y with $A_l=1$, $A_{k\neq l}=0$, that is h_l.

$$Z_{0l}\frac{u(x)}{\epsilon(x)}=\int_0^\infty Z(x,x')h_l(x)dx' \tag{A.19}$$

where H_y is continuous at $x=d$ and

$$Z(x,x')=\frac{1}{2}\cdot\frac{1}{\omega\epsilon_0}\cdot\left\{\sum_{k=1}^{n}\beta_k\frac{u_k(x)}{\epsilon(x)}\frac{u_k(x')}{\epsilon(x')}+\int_0^\infty\left[\beta(\mu)\frac{\phi(x,\mu)}{\epsilon(x)}\frac{\phi(x',\mu)}{\epsilon(x')}+\beta_0(\mu)\psi(x,\mu)\psi(x',\mu)\right]d\mu\right\}. \tag{A.20}$$

Unlike (32) and (64), the μ-integral in the above Green impedance function does not converge in the classical sense. A properly convergent expression, however, can be obtained utilizing a potential function. Let $\Phi(x,\mu)$ be a continuous function, such that

$$\frac{d}{dx}\Phi(x,\mu)=\frac{\phi(x,\mu)}{\epsilon(x)}. \tag{A.21}$$

Then, by partial integration, we have

$$\int_0^\infty\frac{\phi(x,\mu)}{\epsilon(x)}H(x)dx=[\Phi H]_0^\infty-\int_0^\infty\Phi(x,\mu)\frac{dH(x)}{dx}dx. \tag{A.22}$$

If the "trial field" H is a "good" function [20] $\Phi(0,\mu)=0$ and $|\Phi(\infty,\mu)|<\infty$, then the integrated term vanishes. The appropriate function Φ is clearly

$$\Phi(x,\mu)=\sqrt{\frac{2}{\pi}}\frac{1}{sC}\frac{n_2}{n_1^2}\sin sx,\qquad x\leqslant d$$

$$=\sqrt{\frac{2}{\pi}}\left\{\frac{1}{\mu}\frac{1}{n_2}\sin[\mu(x-d)+\alpha]-\frac{n_2}{n_1^2}\frac{v^2}{sC\mu^2}\sin sd\right\},\qquad x\geqslant d. \tag{A.23}$$

In the air space, the appropriate function is

$$\Psi(x,\mu)=\sqrt{\frac{2}{\pi}}\frac{1}{\mu}\sin\mu x. \tag{A.24}$$

As we are dealing with "trial fields" constituted of "good" functions, the Green's impedance function can be rewritten as

$$Z(x,x')=\frac{1}{2}\frac{1}{\omega\epsilon_0}\left\{\sum_k\beta_k\frac{u_k(x)}{\epsilon(x)}\frac{u_k(x')}{\epsilon(x)}+\left(\frac{d}{dx}\right)^T\cdot\int_0^\infty d\mu[\beta(\mu)\Phi(x,\mu)\Phi(x',\mu)+\beta_0(\mu)\Psi(x,\mu)\Psi(x',\mu)]\left(\frac{d}{dx'}\right)\right\} \tag{A.25}$$

where the "transpose" operator $\left(\frac{d}{dx}\right)^T$ is understood to operate on a "good" function of x to the left and $\left(\frac{d}{dx'}\right)$ to the right.

In terms of the basis (37), $\Phi(x,\mu)$ and $\Psi(x,\mu)$ become the vectors $\boldsymbol{R}(\mu)$ and $\boldsymbol{T}(\mu)$ where

$$R_n^{(1)}(\mu)=\sqrt{\frac{\epsilon_n d}{2\pi}}\frac{1}{C}\frac{n_2}{n_1}\frac{2d}{(sd)^2-(n\pi)^2}[1-(-1)^n\cos\alpha d]$$

$$R_n^{(2)}(\mu)=\sqrt{\frac{x_0}{\pi}}\left\{\frac{1}{\mu}\cdot\frac{1}{n_2}\cdot\frac{(-1)^n}{\left(\frac{1}{4}+\mu^2x_0^2\right)^{1/2}}\cdot\sin[(2n+1)\tan^{-1}2\mu x_0+\alpha]-\frac{n_2}{n_1^2}\frac{2v^2}{sC\mu^2}\sin sd(-1)^n\right\} \tag{A.26}$$

$$T_n^{(1)}(\mu)=\sqrt{\frac{2\epsilon nd}{\pi}}\frac{d}{(\mu d)^2-(n\pi)^2}[1-(-1)^n\cos\mu d],\qquad \mu d\neq n\pi$$

$$=0,\qquad \mu d=n\pi$$

$$T_{(n)}^{(2)}(\mu)=\sqrt{\frac{x_0}{\pi}}\frac{1}{\mu}\frac{(-1)^n}{\left(\frac{1}{4}+\mu^2x_0^2\right)^{1/2}}\cdot\sin[(2n+1)\tan^{-1}2\mu x_0+\mu d]. \tag{A.27}$$

Furthermore, the operator $\frac{d}{dx}$ becomes the matrix

$$\underline{\underline{D}}=\begin{pmatrix}D_{1kj} & 0\\ 0 & D_{2mn}\end{pmatrix} \tag{A.28}$$

where

$$D_{1kj}=\int_0^d c_k(x)\frac{d}{dx}c_j(x)dx=\sqrt{\frac{\epsilon_k\epsilon_j}{d}}\,j\left[\frac{(-1)^{j-i}-1}{j-1}+\frac{(-1)^{i+j}-1}{j+i}\right]$$

$$D_{2mn}=\int_d^\infty\mathcal{L}_m(x-d)\frac{d}{dx}\mathcal{L}_n(x-d)dx=\int_0^\infty\mathcal{L}_m(x)\frac{d}{dx}\mathcal{L}_n(x)dx=\frac{1}{x_0}\begin{cases}0, & m>n\\ \frac{1}{2}, & m=n\\ 1, & m<n.\end{cases} \tag{A.29}$$

The integral equation (A.19) for the magnetic field becomes the matrix equation

$$Z_{0l}\tilde{\boldsymbol{Q}}=\underline{\underline{Z}}\cdot\boldsymbol{G}_l \tag{A.30}$$

where

$$\underline{\underline{Z}} = \frac{1}{2\omega_0}\left\{ \sum_{k=1}^{n} \beta_k \tilde{\boldsymbol{Q}}_k \tilde{\boldsymbol{Q}}_k^T + \underline{\underline{\boldsymbol{D}}}^T \cdot \int_0^\infty d\mu \left[\beta(\mu)\boldsymbol{R}(\mu)\boldsymbol{R}^T(\mu) + \beta_0(\mu)\boldsymbol{T}(\mu)\boldsymbol{T}^T(\mu)\right]\cdot \underline{\underline{\boldsymbol{D}}}\right\}. \quad \text{(A.31)}$$

With the above definition, the scattering matrix is given by (65).

Appendix IV

Electric Field Formulation: TE Modes

In the electric field formulation, the reflection coefficient is given by (55), where the unknown $E_x(x)$ is the solution of the integral equation which has the same form as (31) but with the Green's admittance function

$$Y(x,x') = \frac{1}{2\omega\mu_0}\left\{ \sum_k \beta_k u_k(x)u_k(x') + \int_0^\infty \sqrt{n_2^2k_0^2-\mu^2}\ \phi(x,\mu)\phi(x',\mu)d\mu + \frac{2}{\pi}\int_0^\infty d\mu\sqrt{k_0^2-\mu^2}\ \cos\mu x \cos\mu x'\right\}. \quad \text{(A.32)}$$

The above presents a similar convergence problem as (A.30). As a first step towards reducing it to a properly converging form, we rewrite identically the air half-space Green function, the second integral in (A.32), as

$$\tfrac{1}{2}\left(k_0^2 + \frac{d^2}{dx^2}\right)\sum_{\pm} H_0^{(2)}(k_0|x\pm x'|). \quad \text{(A.33)}$$

The limit of the contribution of the region $z<0$ that is the first integral in (A.32) for $v\to 0$, i.e., when this region reduces to a uniform dielectric n_2, is

$$\tfrac{1}{2}\left(n_2^2k_0^2 + \frac{d^2}{dx^2}\right)\sum_{\pm} H_0^{(2)}(n_2k_0|x\pm x'|) \quad \text{(A.34)}$$

whereas, again using partial integration with an unspecified "good" function, the remainder can be cast in the form

$$\left(\frac{d}{dx}\right)^T \int_0^\infty d\mu\sqrt{n_2^2k_0^2-\mu^2}\ t(x,x';\mu)\left(\frac{d}{dx'}\right) \quad \text{(A.35)}$$

where

$$t(x,x';\mu) = \Phi(x,\mu)\Phi(x',\mu) - \frac{2}{\pi}\frac{1}{\mu^2}\sin\mu x \sin\mu x' \quad \text{(A.36)}$$

$$\Phi(x,\mu) = \sqrt{\frac{2}{\pi}}\ \frac{1}{sC}\sin sx, \qquad 0\leqslant x\leqslant d$$

$$= \sqrt{\frac{2}{\pi}}\left\{\frac{1}{\mu}\sin[\mu(x-d)+\alpha] - \frac{v^2}{Cs\mu^2}\sin sd\right\}, \qquad d\leqslant x. \quad \text{(A.37)}$$

Hence the Green's admittance can be written as

$$Y(x,x') = \frac{\omega\mu_0}{2}\left\{ \sum_k \beta_k u_k(x)u_k(x') + \frac{1}{2}\left(n_2^2k_0^2 + \frac{d^2}{dx^2}\right)\cdot\sum_{\pm} H_0^{(2)}(x_2k_0|x\pm x'|) + \frac{1}{2}\left(k_0^2+\frac{d^2}{dx^2}\right)\sum_{\pm} H_0^{(2)}(k_0|x\pm x'|) + \int_0^\infty d\mu\sqrt{n_2^2k_0^2-\mu^2}\ t(x,x';\mu)\right\}. \quad \text{(A.38)}$$

The integral equation for the electric field $E_l(x)(A_l=1, A_{k\neq l}=0)$ becomes the matrix equation

$$Y_{0l}\boldsymbol{Q} = \underline{\underline{\boldsymbol{Y}}}\cdot\boldsymbol{F}_l \quad \text{(A.39)}$$

where

$$\underline{\underline{\boldsymbol{Y}}} = \frac{1}{2\omega\mu_0}\left\{ \sum_k \beta_k \boldsymbol{Q}_k\boldsymbol{Q}_k^T + n_2^2k_0^2\,\underline{\underline{\boldsymbol{H}}}(n_2k_0) + k_0^2\,\underline{\underline{\boldsymbol{H}}}(k_0) + \underline{\underline{\boldsymbol{D}}}^T\cdot\left[\underline{\underline{\boldsymbol{H}}}^+(n_2k_0) - \underline{\underline{\boldsymbol{H}}}^-(n_2k_0) + \underline{\underline{\boldsymbol{H}}}^+(k_0) - \underline{\underline{\boldsymbol{H}}}^-(k_0) + \int_0^\infty d\mu\sqrt{n_2^2k_0^2-\mu^2}\left[\boldsymbol{R}(\mu)\boldsymbol{R}^T(\mu) - \boldsymbol{T}(\mu)\boldsymbol{T}^T(\mu)\right]\right]\cdot\underline{\underline{\boldsymbol{D}}}\right\}. \quad \text{(A.40)}$$

It is required to evaluate the matrix elements

$$I_{mn} = \iint_0^\infty dxdx' L_m(x)\frac{d^2}{dx^2}\tfrac{1}{2}\sum_{\pm} H_0^{(2)}[k_0|x\pm x'|]L_n(x'). \quad \text{(A.41)}$$

As

$$\frac{d^2}{dx^2}H_0^{(2)}[k_0|x\pm x'|] = \pm\frac{d}{dx}\frac{d}{dx'}H_0^{(2)}[k_0(x\pm x')] \quad \text{(A.42)}$$

we have

$$I_{mn} = \left[\underline{\underline{\boldsymbol{D}}}^T\cdot\left(\underline{\underline{\boldsymbol{H}}}_{mn}^{+} - \underline{\underline{\boldsymbol{H}}}_{mn}^{-}\right)\cdot\underline{\underline{\boldsymbol{D}}}\right].$$

Acknowledgment

The authors wish to express their thanks to Dr. W. P. A. Joosen for providing the important result (A.14) in Appendix II, as well as to Ir. P. de Waard for his useful comments.

References

[1] C. Angulo, "Diffraction of surface waves by a semi-infinite dielectric slab," *IRE Trans., Antennas Propagat.*, vol. AP-5, pp. 100–109, Jan. 1957.

[2] T. Ikegami, "Reflectivity of mode at facet and oscillation mode in double-heterostructure injection lasers," *IEEE J. Quantum Electron.*, vol. QE-6, pp. 470–476, June 1972.

[3] G. A. Hockham and A. B. Sharpe, "Dielectric waveguide discontinuities," *Electron. Lett.*, vol. 8, pp. 230–231, May 1972.

[4] F. K. Reinhart, I. Hayashi, and M. Panish, "Mode reflectivity and waveguide properties of double-heterostructure injection lasers," *J. Appl. Phys.*, vol. 42, no. 11, pp. 4466–4479, Oct. 1971.

[5] J. K. Butler and J. Zoroofchi, "Radiation fields of GaAs injection lasers," *J. Quantum Electron.*, vol. QE-10, pp. 809–815, Oct. 1974.

[6] L. Lewin, "A method for the calculation of the radiation-pattern

and mode-conversion properties of a solid-state heterojunction laser," *IEEE Trans. Microwave Theory Tech.*, vol. MTT-23, pp. 576–585, July 1975.
[7] H. Kressel and J. K. Butler, *Semiconductor Lasers and Heterojunction LEDs* New York: Academic, 1977, ch. 5.
[8] H. C. Casey and M. B. Panish, *Heterostructure Lasers*. New York: Academic, 1978, ch. 2.
[9] T. Rozzi, "Rigorous analysis of the step discontinuities in planar dielectric waveguides," *IEEE Trans. Microwave Theory Tech.*, vol. MTT-26, pp. 738–746, Oct. 1978.
[10] T. Rozzi and G. in't Veld, "Field and network analysis of interacting step discontinuities in planar dielectric waveguides," *IEEE Trans. Microwave Theory Tech.*, vol. MTT-27, pp. 303–309 Apr. 1979.
[11] E. A. J. Marcatili, "Dielectric rectangular waveguide and directional coupler for integrated optics," *Bell. Syst. Tech. J.*, vol. 48, pp. 2071–2102, Sept. 1969.
[12] T. Rozzi, T. Itoh, and L. Grun, "Two-dimensional analysis of the GaAs d.h. stripe-geometry laser," *Rad. Sci.*, vol. 12, no. 4, pp. 543–549, July-Aug. 1977.
[13] E. I. Gordon, "Mode selection in GaAs injection lasers resulting from Fresnel reflection," *IEEE J. Quantum Electron.*, vol. QE-9, pp. 772–776, July 1973.
[14] P. J. Waard, "Calculation of the far field half power width and mirror reflection coefficients of d.h.-lasers," *Electron. Lett.*, vol. 11, no. 1, pp. 11–12, Jan. 9, 1975.
[15] L. Lewin, "Obliquity factor for radiation from solid-state lasers," *Electron. Lett.*, vol. 10, no. 8, pp. 136–138, Apr. 18, 1974.
[16] H. C. Casey et al., "Beam divergence of the emission from d.h. injection lasers," *J. Appl. Phys.*, vol. 12, pp. 5470–5475, Dec. 1973.
[17] G. Acket, private communication.
[18] P. A. Kirkby et al., "Observation of self-focusing in stripe geometry semiconductor lasers...," *IEEE J. Quantum Electron.*, vol. QE-13, pp. 705–719, Aug. 1977.
[19] I. S. Gradshteyn and I. M. Ryshik, *Tables of Integrals, Series and Products*. New York: Academic, 1965.
[20] M. Lighthill, *Generalized Functions and Fourier transforms. Cambridge, MA: Univ. Press*, 1962.

Transmission-Line Conductors of Various Cross Sections

HAROLD A. WHEELER, FELLOW, IEEE

Abstract—**The inner or outer conductor of an RF transmission line may have a noncircular shape of cross section, in which case it can be ascribed an effective radius which is valid if the two conductors are sufficiently separated (as by the ratio of radii). Moreover, there are some combinations of inner and outer conductors whose wave resistance can be evaluated exactly. These can be used to test the degree of approximation of the effective radii. There are some unique shapes of combinations which have binary submultiples of 377 ohms wave resistance because the field pattern of each can be mapped on a set of squares. A variety of cross sections are described and evaluated, with due reference to their sources. They are related by conformal transformations, which are indicated but not derived. One example is an inner conductor whose cross section is a rectangle with rounded edges. One family is based on the crescent or biangle formed of two circular arcs between two angles.**

I. Introduction

An RF TRANSMISSION line is formed of two cylindrical conductors, typically an inner conductor shielded by an outer conductor which provides the return circuit.

The properties of either conductor depend on its cross section, which is described by its size and shape. Here it is taken to be made of a perfect conductor so the skin depth approaches zero at the operating (high) frequency. Then its boundary is the same toward electric or magnetic field. Also the significant dimensions of its cross section are taken to be such a small fraction of the wavelength that the TEM mode is the only field pattern that need be considered.

Manuscript received June 4, 1979.
The author is with the Hazeltine Corporation, Greenlawn, NY 11740.

The two conductors may be separated sufficiently (as by a large ratio of size) that each can be evaluated in terms of an equivalent circular cross section. Then the effective radius of either one is defined as the radius of the equivalent circle. The intervening space contains a region where the field configuration is nearly independent of the peculiarities of the shape of either cross section. This concept is valid as an approximation for a wide variety of shapes that have practical and/or academic interest. Any one shape is related to the equivalent circle by a conformal transformation that may be susceptible of simple formulation.

The evaluation of a shape in terms of its effective radius is here expressed by stating the dimensions equivalent to a unit radius. This is the viewpoint of synthesis, and can easily be reversed for analysis.

The most common conformal transformation is the algebraic integral power or root about some origin, which preserves the unit circle as a reference. Inversion in a unit circle transforms from an inner conductor to an outer conductor, or vice versa.

If the two conductors are not sufficiently separated, so there is some interaction of their shapes, a rigorous evaluation must be based on the composite shape of the double conductor. This incidentally provides some examples for testing the degree of approximation enabled by the separate effective radii.

The dielectric medium is taken to be free space.

There are presented here a variety of shapes of conduc-

0018-9480/80/0200-0073$00.75 ©1980 IEEE